Supporting Information

Fe/N-Doped Porous Carbon Spheres Enable $^{\bullet}OH$-to-$^{1}O_2$ Mechanism Shift for Selective Sulfonamide Degradation in High-Salinity Wastewater via Low-Temperature Plasma

Chenyu Zhao[a1], Mei Li[b1], Yu Liu[a], Lei Sun[a], Jingwen Min[a], Ying Cao[a], Wuxiang Zhang[c], Weichuan Qiao[a], Ming Zhang[a]*

a) Department of Environmental Engineering, College of Ecology and Environment, Nanjing Forestry University, Nanjing 210037, PR China.

b) Nanjing Institute of Environmental Sciences, Ministry of Ecology and Environment of the People's Republic of China, Nanjing, China.

c) School of Environmental and Chemical Engineering, Jiangsu University of Science and Technology, Zhenjiang 212003, PR China.

Text, Table, and Figure of catalogues

Text S1 Experimental setup P4

Text S2 Characterization P5

Text S3 Determination of organic matter concentration P6

Text S4 Analytical methods P7

Text S5 Toxicity evaluation P8

Table S1 The content of S_{BET}, V_{pore} and the pore size P9

Table S2 The comparison of performance of different catalysts P10

Table S3 HPLC detection conditions of different contaminants P11

Table S4 The XPS spectral analysis of element content changes ASC and 0.4MFe/ASC P12

Table S5 The Fukui functions of SMT P13-14

Table S6 The Fukui functions of SMX P15-16

Table S7 The Fukui functions of SD P17-18

Table S8 Several intermediates and m/z values were detected by LC-MS in MMFeP-800℃+NaCl/DBD system P19

Fig S1 Schematic diagram of experimental setup P20

Fig S2 SEM patterns of different catalysts P21

Fig S3 Degradation rates, adsorption profiles, k and adsorption capacity of TTCH under DBD alone and with different catalysts P22

Fig S4 Effect of different conditions on degradation rate P23

Fig S5 (a) Energy efficiency and G_{50} of different system, (b)EE/O of different systems. P24

Fig S6 The steady-state concentrations of •OH, and $^1O_2$ P25

Fig S7 Effects of bursting agents and k of bursting agents in DBD system P26

Fig S8 Effects of bursting agents and k of bursting agents in MMFeP-800 ℃/DBD system P27

Fig S9 Effects of bursting agents and k of bursting agents in NaCl/DBD system P28

Fig S10 The concentration of H_2O_2 in different system P29

Fig S11 (a) Effects of bursting agents KSCN, (b) The effect of sonked MMFeP-800 ℃ P30

Fig S12 Degradation rates of SMT with different salt P31

Fig S13 Reflected rates under DBD alone and with MMFeP-800 ℃, Na_2SO_4, KCl P32

Fig. S14 (a) The change of pH during the reaction in NaCl, (b) Effects of bursting agents $Na_2S_2O_3$ P33

Fig S15 Effect of 5 mM HA and 5 mM $NaHCO_3$ on the degradation of SMT. P34

Fig S16 The LC-MS results of intermediates in MMFeP-800 ℃/NaCl/DBD P35

Fig S17 The LC-MS results of intermediates in MMFeP-800 ℃/NaCl/DBD P36

Fig S18 The LC-MS results of major retention times P37

Fig S19 Toxicity evaluation of SMT and its degradation intermediates P38

Text S1 Experimental setup

The experimental system is depicted in Fig. 1. Dielectric barrier discharge is applied to stimulate the low-temperature plasma. Quartz glass with 1 mm is the dielectric barrier between the reaction mixture and electrode. The power supply (PSPT-2000K) was obtained from Nanjing Perspet Electronic Technology Co. During the experiment, the solution to be treated flowed into the reactor through a longer pump (YZ1515x) at a flow rate of 45 mL/min. The diameter of the reactor was 7 cm, the height was 4 cm, and the wall thickness was 2 mm. The catalyst was placed in the reactor. The water treatment capacity at the time was 100 mL. The treated solution flowed back to the beaker and was mixed well under the action of a magnetic stirrer, and then entered the reactor through a longer pump for circulating treatment.

Test S2 Characterization

The field emission scanning electron microscope (SEM) (JEOL 7800F) and field emission transmission electron microscope (TEM) (FEI Tecnai 20) were used to characterize the morphology, size and internal structure of the catalysts. X-ray diffraction (XRD) (BRUKER D8) was used to characterize the crystal structures of the synthesized precursors and their derivatives using Cu Ka radiation in the range of 5◦ to 80◦ with a resolution of 0.02 min^{-1} scan rate. The fourier transform infrared (FTIR) (VERTEX 80 V, BRUKER) was used to determine the surface functional groups of the catalysts. The specific surface area porosity analyzer (S_{BET}) (ASAP2460, Micromeritics) was used to test the specific surface area as well as the pore size distribution of the materials in liquid nitrogen. The x-ray photoelectron spectroscopy (XPS) (PHI Quantera II ESCA system) was used to investigate the elemental composition of the catalysts under Al Kα radiation at 1486.8 V

Text S3 Determination of organic matter concentration

The concentrations of acid orange 7 (AO7), methylene blue (MB) and Oxytetracycline (OTC) were determined by a UV spectrophotometer. The absorption wavelengths were 484 nm, 664 nm and 355 nm, respectively. For the determination of the concentrations of the organics tetracycline (TTCH), bisphenol A (BPA), sulfamethazine (SMT), Sulfamethoxazole (SMX), Sulfadiazine(SD) and Ofloxacin(OFX), a High-Performance Liquid Chromatography (HPLC, UltiMate 3000) equipped with a C18 column was used. Before the determination, 1 mL of the sample solution to be measured was added to 1 mL of methanol, mixed thoroughly, and filtered through a 0.22 μm organic phase filter into a sample vial. The injection volume of all samples was 20 μL, and the HPLC test parameters were detailed in Table S4

Text S4 Analytical methods

(1) Degradation efficiency of TTCH (%) analysis

The calculation of the degrading efficiency of TTCH can be determined using Eq. (1):

$$Degradation\ efficiency\ of\ TTCH\ (\%) = \frac{C_0 - C}{C_0} \times 100\% \quad (1)$$

where C_0 is the initial concentration of TTCH, and C is the instantaneous concentration of TTCH.

The pseudo-first-order kinetics model was used to determine the reaction rate constants (k) of TTCH degradation under various conditions:

$$-\ln\left(\frac{C}{C_0}\right) = kt \quad (2)$$

(2) Energy yield analysis

According to Eq. (3), the energy yield (EY) represents the mass of the TTCH degradation unit of energy consumed:

$$EY(g/k\ Wh) = \frac{C_0(g/L) \times \eta(\%) \times V(L)}{P(kW) \times t(h)} \times \frac{1}{100} \quad (3)$$

The G_{50} value represents the energy efficiency of the degradation process when the concentration of TTCH is decreased to 50% of its initial concentration, as indicated in Equation (4).

$$G_{50}(g/k\ Wh) = \frac{C_0(g/L) \times V(L) \times 50}{P(kW) \times t_{50}(h)} \times \frac{1}{100} \quad (4)$$

where C_0 is the initial concentration of TTCH, η is the TTCH degradation efficiency, P is the discharge power, V is the treatment volume, and t is the treatment time.

(3) The Hindrance efficiency ξ (%) analysis

The Hindrance efficiency ξ (%) of the scavenger agents on TTCH elimination is calculated as Eq. (5):

$$\xi\ (\%) = \frac{k_0 - k}{k_0} \times 100\% \quad (5)$$

where k_0 and k are the pseudo-first-order kinetics constants without the scavenger agents (min^{-1}) and with the addition of scavengers (min^{-1}), respectively.

Test S5 Toxicity evaluation

SMT, degradation products, and materials were evaluated for toxicity using E. coli growth inhibition bioassays. E. coli BL121 (DE3) was added to 50 mL of Luria-Bertani (LB) medium and activated at 37 °C for 12 h. And 1.0 mL of cultured E. coli liquid was inoculated into solid LB medium to effect the growth of E. coli. Then, 10 mL of TTCH at a concentration of 20 mg/L, the degradation product, and a certain amount of material were added to observe the growth of E. coli. It was shown the toxicity of the TTCH, degradation products and the materials.

Table S1 The content of S_{BET}, V_{pore} and the pore size

Sample	$S_{BET}(m^2/g)$	$V_{pore}(cm^3/g)$	Pore Size(nm)
MP-800℃	341.93	0.25	2.88
MMFeP-700℃	286.72	0.30	4.14
MMFeP-800℃	465.15	0.50	4.30
MMFeP-900℃	429.65	0.51	4.76

Table S2 The comparison of performance of different catalysts

Catalyst	Pollutant (ppm)	Catalyst dosage(g/L)	Remove efficiency (%)	Ref.
Fe_3O_4	CAP (20)	0.26	80.5	(Guo et al., 2020)
nFe(0)/BC	TTCH (100)	0.2	87.85	(Shao et al., 2020)
Fe-Mn/AC	TTCH (50)	0.5	98.8	(A et al., 2021)
ZVI (Fe^0)	AO7 (63)	26	80	(Du et al., 2010)
MMFeP-800℃	SMT (50)	0.15	99.03	This work

Table S3 HPLC detection conditions of different contaminants

Contaminants	Detection wavelength	Mobile phase	Flow rate
Tetracycline (TTCH)	355 nm	Acetonitrile: DI (20:80,v/v)	0.3 mL/min
Sulfamethoxazole (SMX)	265 nm	Acetonitrile: 0.1% Formic acid (40:60,v/v)	0.8 ml/min
Sulfadiazine (SD)	270 nm	Methanol: DI (35:65,v/v)	1.0 mL/min
Bisphenol A (BPA)	230 nm	Methanol: DI (20:80,v/v)	1.0 mL/min
Ofloxacin (OFX)	288 nm	Acetonitrile: 0.1% Formic acid (30:70,v/v)	1.0 mL/min
Sulfamethazine (SMT)	270 nm	Methanol: DI (35:65,v/v)	1.0 mL/min

Table S4 The XPS spectral analysis of element content changes ASC and 0.4MFe/ASC.

Sample	C	N	O	Fe
Before reaction	77.22 %	4.54 %	15.67 %	2.57 %
After reaction	66.95 %	4.43 %	21.85 %	6.77 %

Table S5 The Fukui functions of SMT

SMT			
Atom (number)	f_k^-	f_k^+	f_0
C1	-0.35131	-0.2213	-0.27914
C2	0.16908	0.17776	0.16603
C3	-0.36064	-0.21175	-0.27994
C4	-0.26863	-0.20731	-0.20182
C5	-0.37611	-0.30299	-0.39614
C6	-0.28972	-0.20919	-0.2056
S7	2.35548	2.34707	2.35524
O8	-0.93292	-0.87098	-0.90698
O9	-0.93245	-0.87378	-0.9087
N10	-0.85933	-0.85141	-0.85757
C11	0.58743	0.58354	0.58876
N12	-0.61561	-0.42913	-0.53411
C13	0.18088	0.27935	0.26557
C14	-0.33808	-0.31072	-0.34478
C15	0.16216	0.28609	0.27273
N16	-0.5752	-0.41634	-0.52392
C17	-0.6801	-0.71066	-0.70246
C18	-0.67944	-0.7099	-0.70053
N19	-0.79832	-0.65561	-0.78566
H20	0.19651	0.25844	0.22907
H21	0.19563	0.25862	0.22869
H22	0.23534	0.28723	0.26108
H23	0.23547	0.28512	0.26018
H24	0.46096	0.46607	0.46367
H25	0.20159	0.26432	0.23442
H26	0.20344	0.25341	0.22843

H27	0.22154	0.27475	0.25623
H28	0.22137	0.27563	0.25658
H29	0.20695	0.25548	0.23144
H30	0.21622	0.26847	0.25018
H31	0.21857	0.26795	0.25074
H32	0.39448	0.44592	0.41427
H33	0.39478	0.44584	0.41406

Table S6 The Fukui functions of SMX

SMX			
Atom (number)	f_k^-	f_k^+	f_0
C1	-0.39069	-0.19644	-0.19159
C2	-0.33383	-0.23086	-0.29106
C3	0.13927	0.20482	0.19076
C4	-0.40463	-0.23381	-0.29148
C5	-0.1903	-0.17918	-0.17892
C6	-0.42869	-0.32769	-0.39193
S7	2.31718	2.32537	2.34215
O8	-1.00067	-0.91998	-0.96019
O9	-0.98906	-0.89153	-0.94935
N10	-0.84914	-0.77578	-0.84401
C11	0.31569	0.33389	0.31074
C12	-0.39201	-0.38714	-0.39333
C13	0.3042	0.42437	0.35083
O14	-0.34094	-0.27983	-0.31224
N15	-0.26397	-0.04431	-0.21854
C16	-0.72172	-0.74965	-0.73268
N17	-0.81056	-0.68367	-0.78029
H18	0.20871	0.27341	0.25616
H19	0.18971	0.2616	0.23528
H20	0.19254	0.26346	0.23626
H21	0.23891	0.29524	0.27405
H22	0.43458	0.47056	0.44876
H23	0.27121	0.29837	0.27616
H24	0.23716	0.27863	0.25433
H25	0.24356	0.28776	0.25975
H26	0.24398	0.28771	0.25982

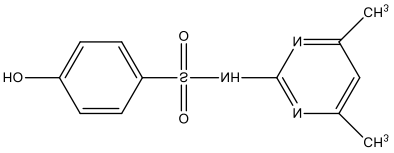
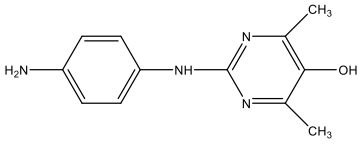
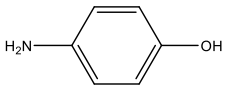
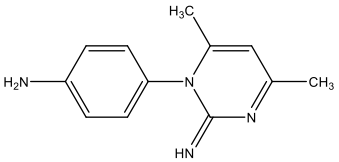
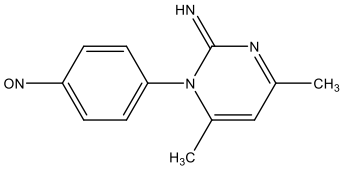
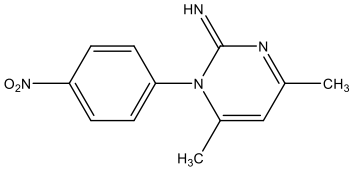
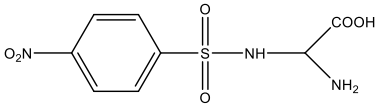
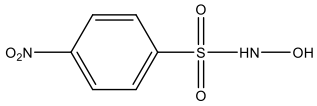
H27	0.38856	0.44788	0.42058
H28	0.39096	0.44679	0.41997

Table S7 The Fukui functions of SD

SD			
Atom (number)	f_k^-	f_k^+	f_0
C1	-0.33611	-0.199	-0.19435
C2	-0.34806	-0.23819	-0.29343
C3	0.16962	0.20318	0.18829
C4	-0.39203	-0.24049	-0.29259
C5	-0.20755	-0.17909	-0.17946
C6	-0.39586	-0.33555	-0.39151
S7	2.33693	2.32186	2.34177
O8	-0.97895	-0.90558	-0.9481
O9	-0.96682	-0.87303	-0.93642
N10	-0.8348	-0.74949	-0.83365
C11	0.36785	0.39103	0.37227
C12	-0.34729	-0.2317	-0.31345
C13	-0.27341	-0.18725	-0.18505
C14	-0.33638	-0.21027	-0.32477
C15	-0.00516	0.08068	0.04771
N16	-0.54066	-0.44216	-0.4794
N17	-0.80286	-0.69511	-0.78256
H18	0.2202	0.26821	0.25275
H19	0.19577	0.25781	0.23262
H20	0.19829	0.26063	0.23453
H21	0.24734	0.29403	0.2744
H22	0.42645	0.46378	0.44136
H23	0.20104	0.25231	0.22516
H24	0.20672	0.27296	0.23962
H25	0.20804	0.27218	0.23938
H26	0.19676	0.2594	0.22706

H27	0.39501	0.44522	0.41947
H28	0.3959	0.44359	0.41837

Table S8 Several intermediates and m/z values were detected by LC-MS in MMFeP-800℃+NaCl/DBD system

Detected Intermediates	Chemical structure	Molecular weight (MW)	Detected m/z
P1		280	280.45
P2		229	229.57
P3		108	108.06
P4		215	213.39
P5		230	229.37
P6		246	246.11
P7		274	274.25
P8		218	218.39
P9		112	111.97

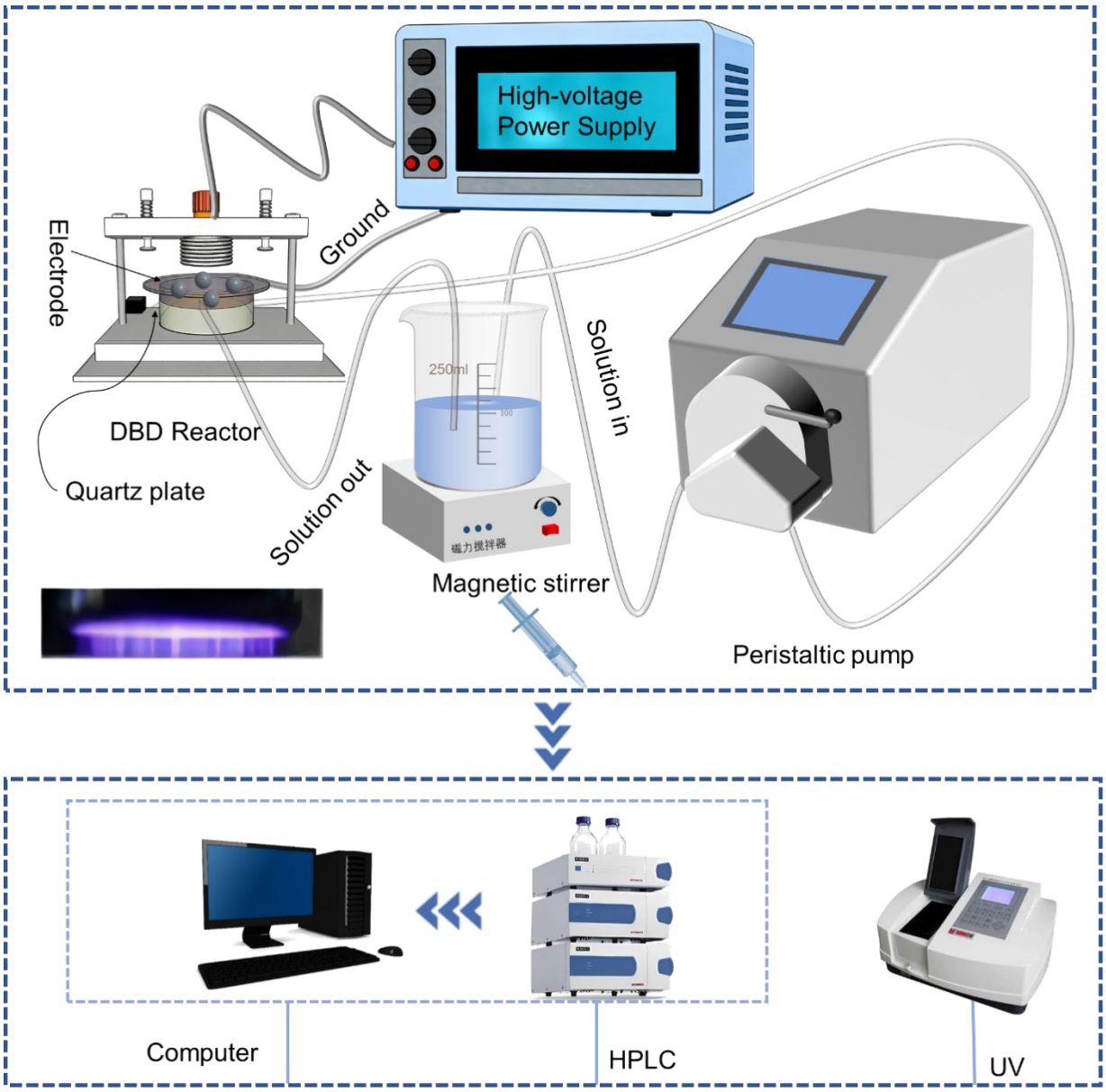


Fig. S1 Schematic diagram of experimental setup.

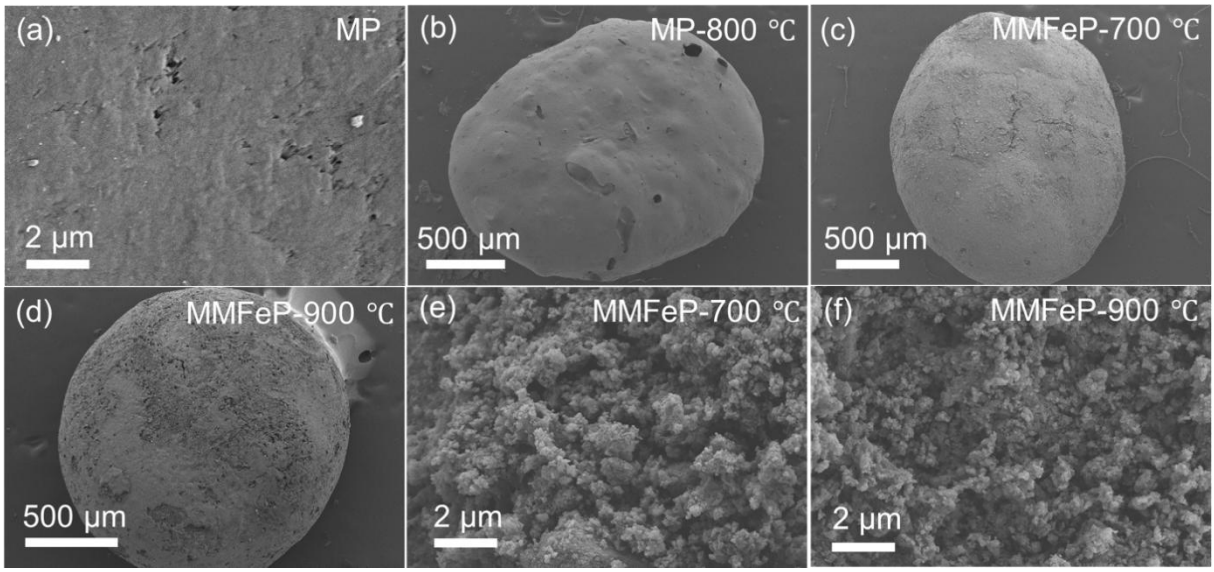


Fig. S2 SEM patterns of catalysts (a) MP, (b) MP-800 ℃, (c) MMFeP-700 ℃, (d) MMFeP-900 ℃, (e) MMFeP-700 ℃, (f) MMFeP-900 ℃.

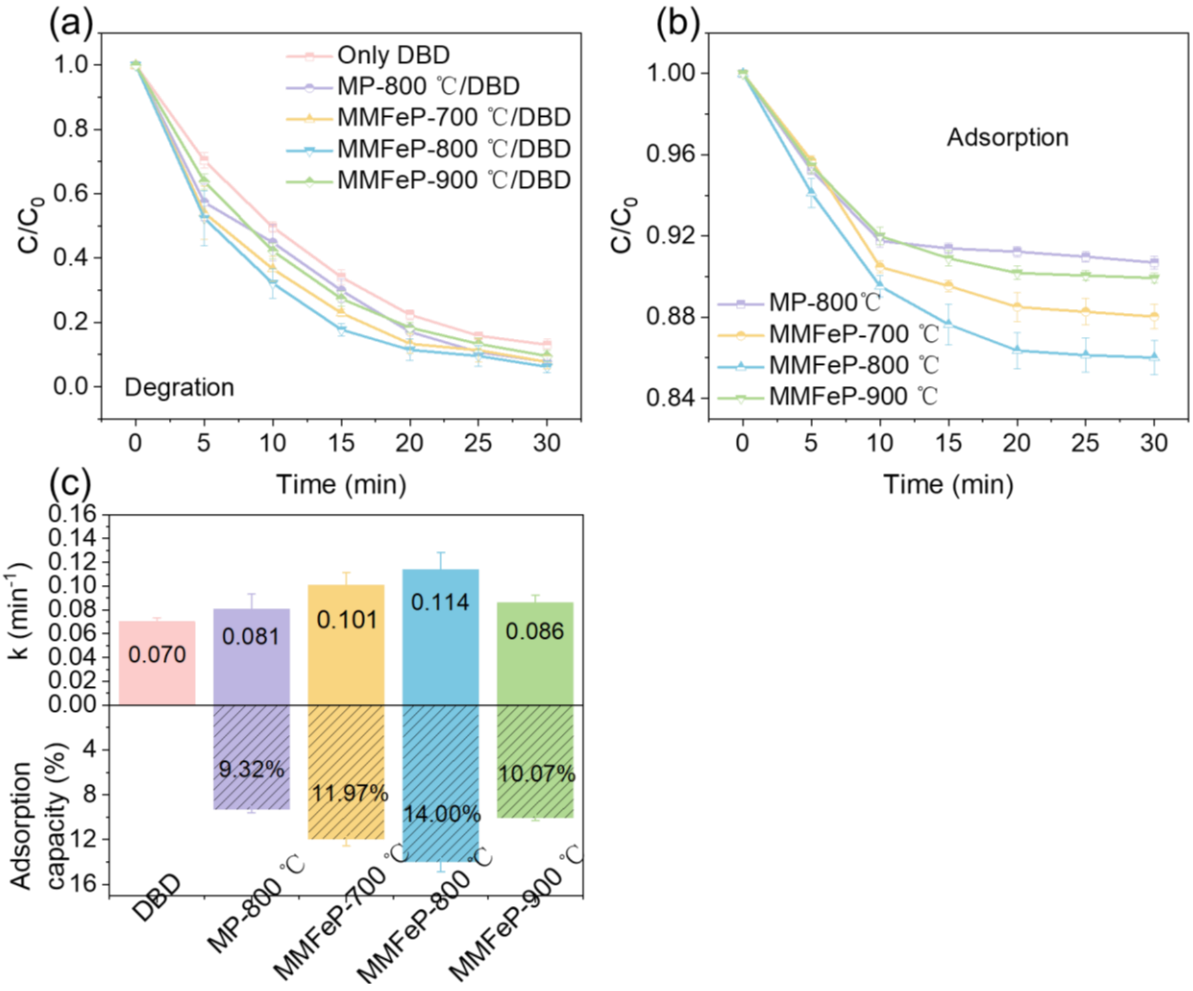


Fig. S3 (a) Degradation rates of TTCH under DBD alone and with different catalysts; (b) Adsorption profiles of different catalysts; (c) Reflected rates and adsorption capacity under DBD alone and with different catalysts.

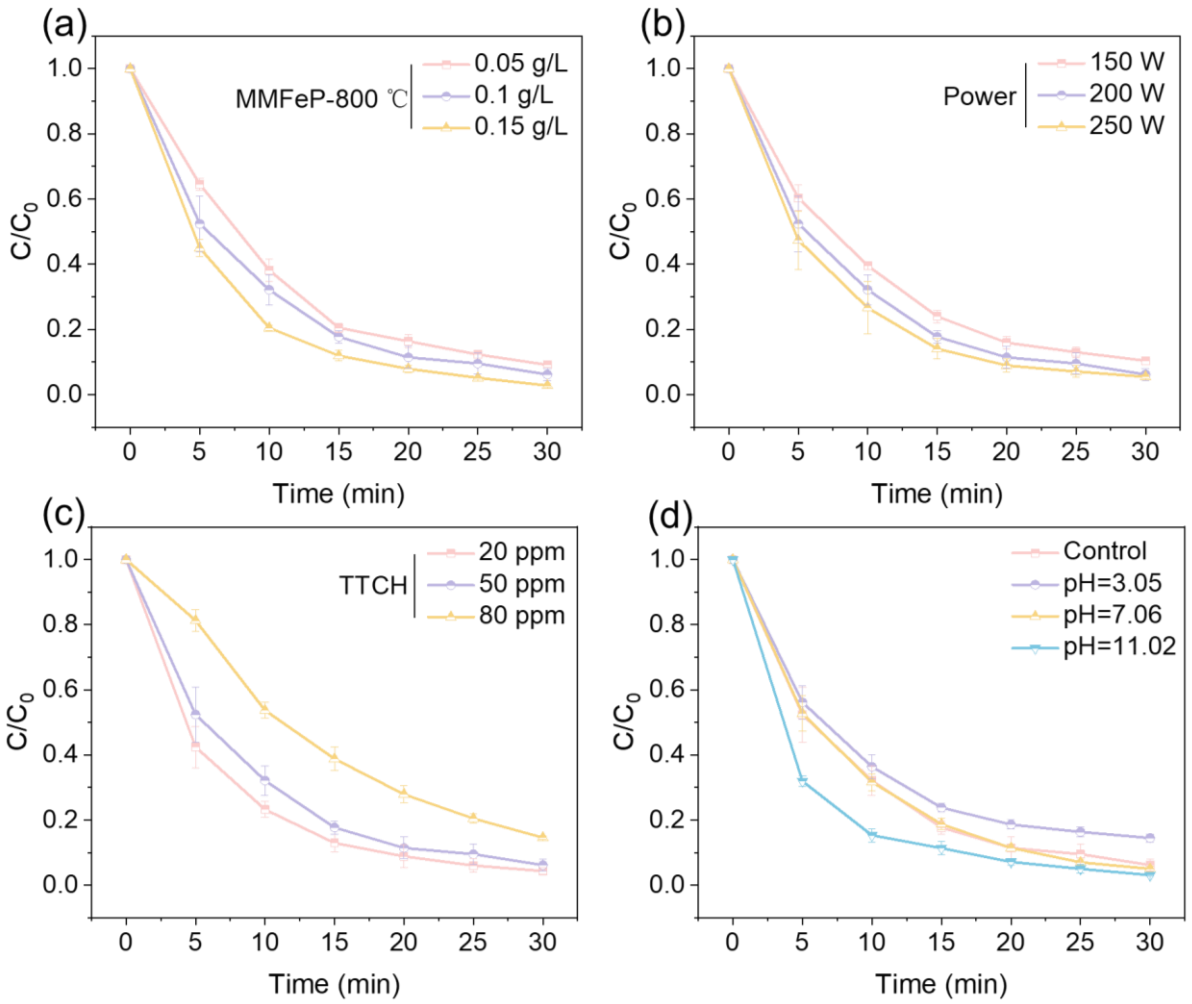


Fig. S4 (a) Effect of catalyst dosage on degradation rate; (b) Effect of power on degradation rate; (c) Effect of TTCH concentration on degradation rate; (d) Effect of different pH on degradation rate.

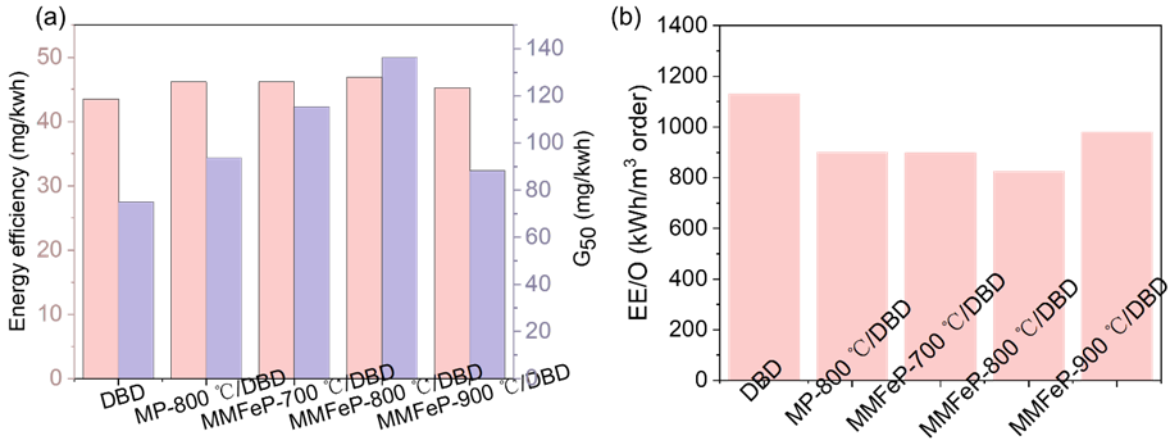


Fig. S5 (a) Energy efficiency and G_{50} of different systems, (b)EE/O of different systems.

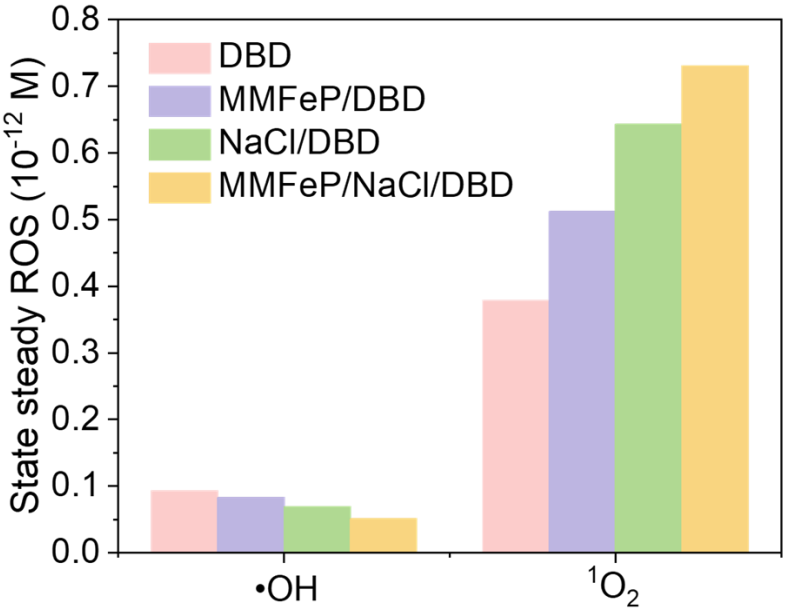


Fig. S6 The steady-state concentrations of •OH, and $^1O_2$

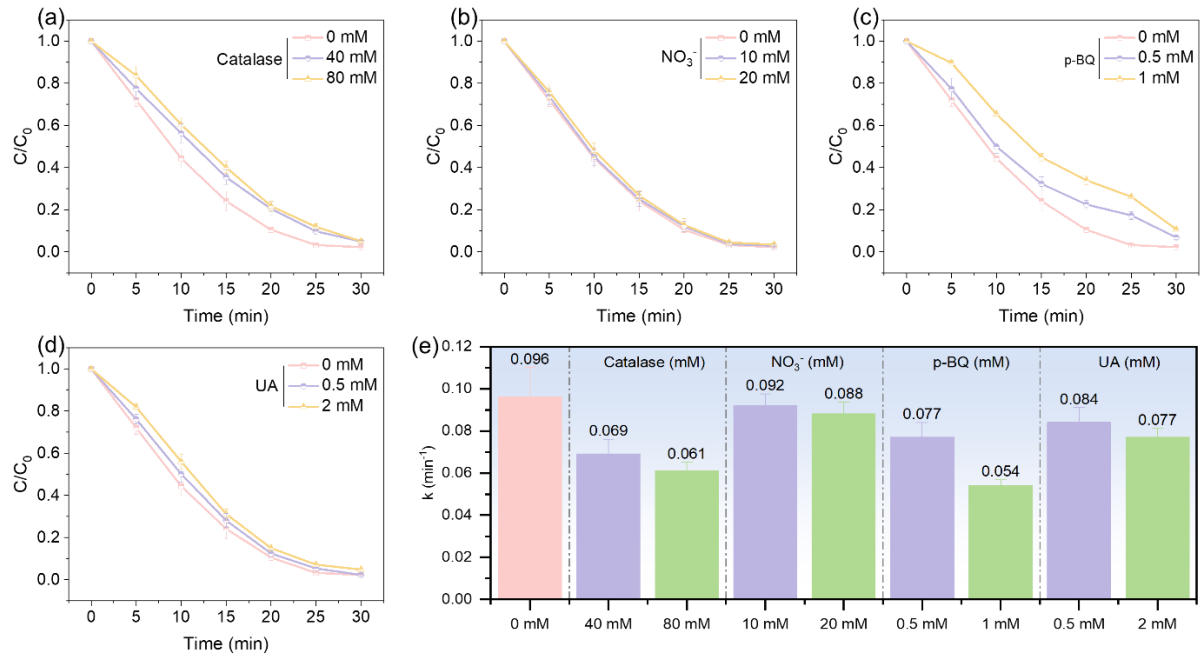


Fig. S7 Effects of bursting agents (a) Catalase, (b) NO_3^-, (c) p-BQ, (d) UA, (e) Reflected rates of bursting agents in DBD.

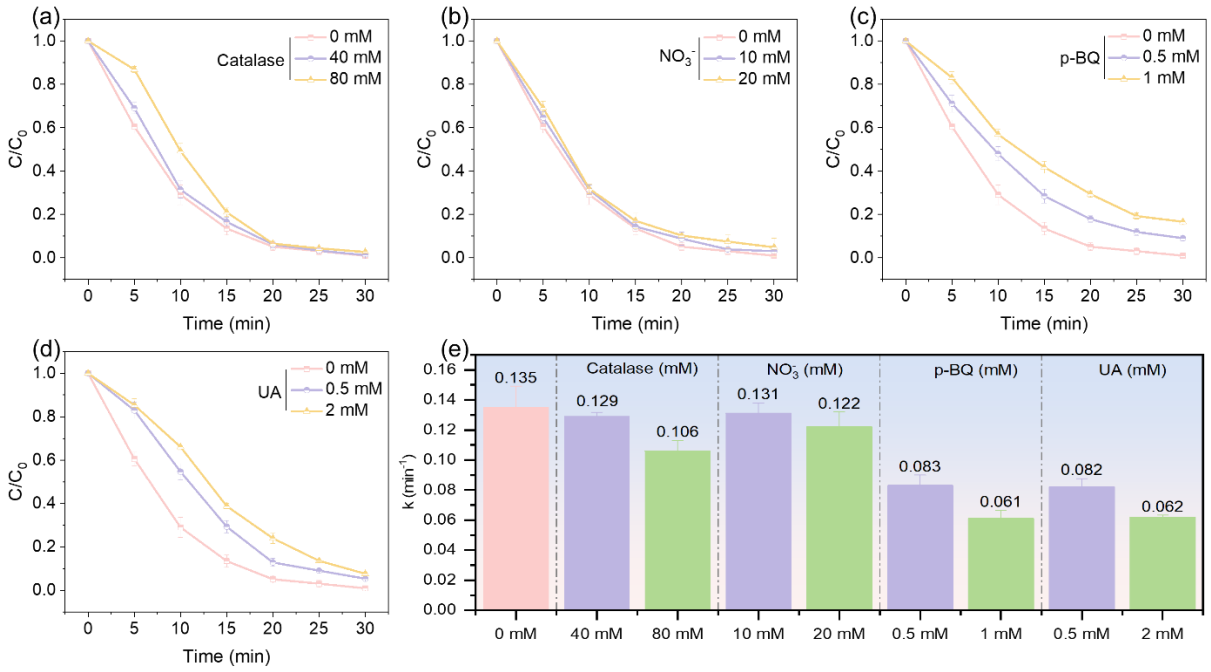


Fig. S8 Effects of bursting agents (a) Catalase, (b) NO_3^-, (c) p-BQ, (d) UA, (e) Reflected rates of bursting agents in MMFeP-800 ℃/DBD.

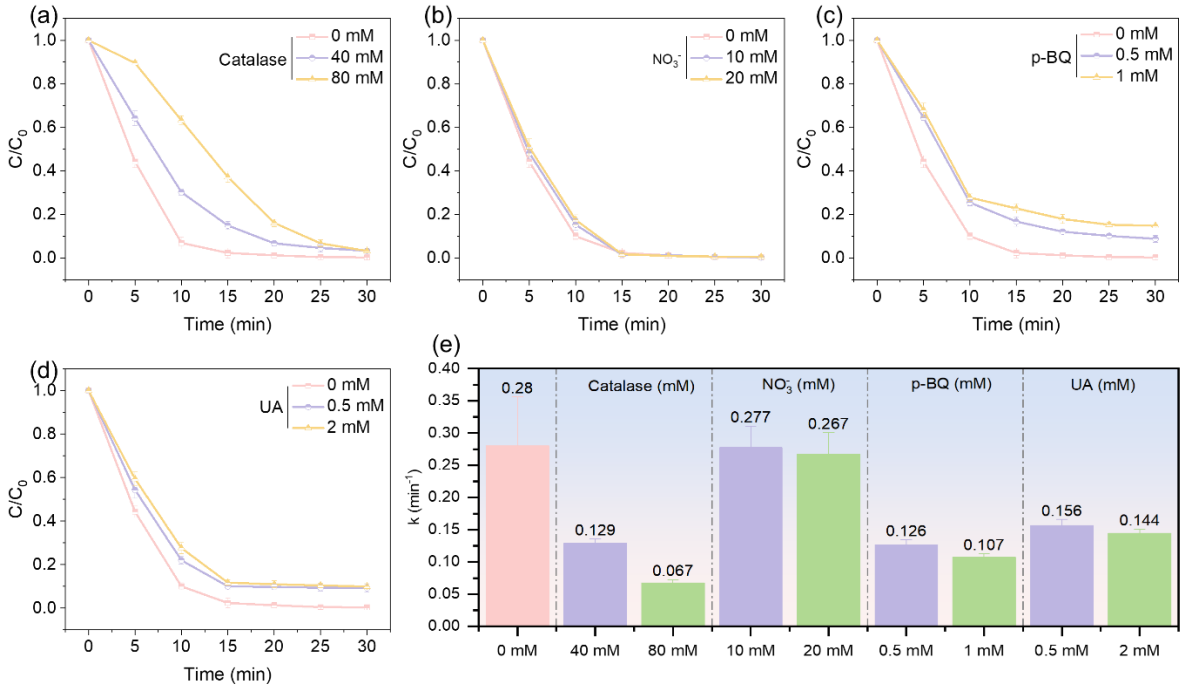


Fig. S9 Effects of bursting agents (a) Catalase, (b) NO_3^-, (c) p-BQ, (d) UA, (e) Reflected rates of bursting agents in NaCl/DBD.

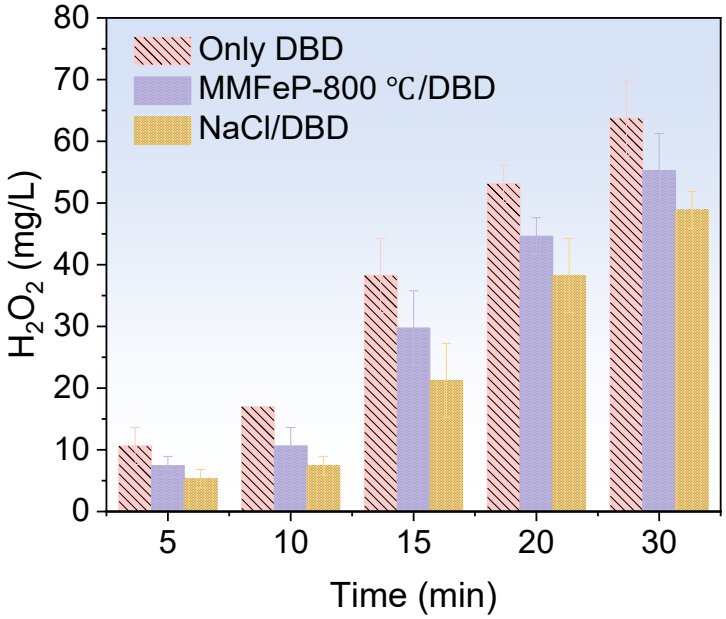


Fig. S10 The concentration of H_2O_2 in different system.

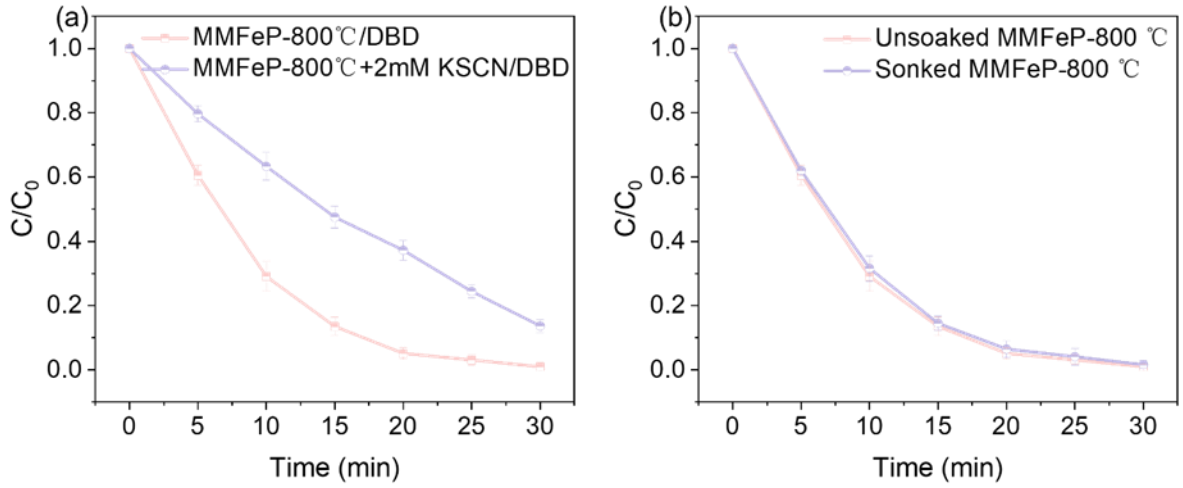


Fig. S11 (a) Effects of bursting agents KSCN, (b) The effect of sonked MMFeP-800 ℃

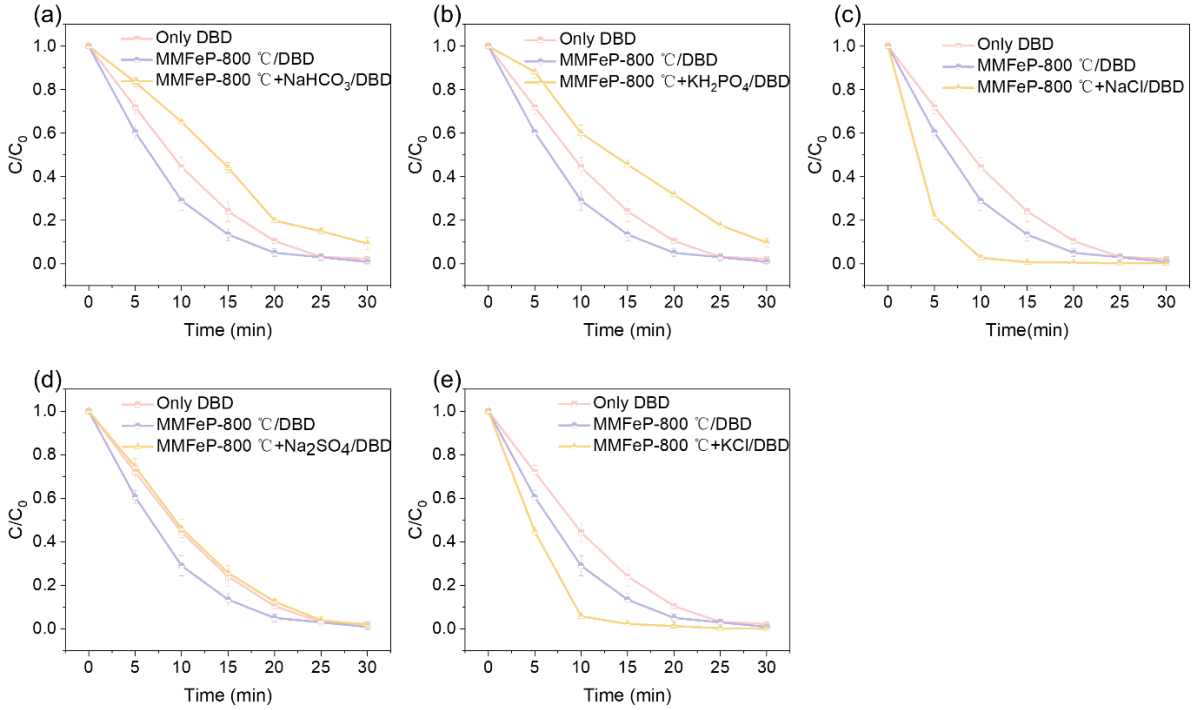


Fig. S12 Degradation rates of SMT with (a) $NaHCO_3$, (b) KH_2PO_4, (c) NaCl, (d) Na_2SO_4, (e) KCl.

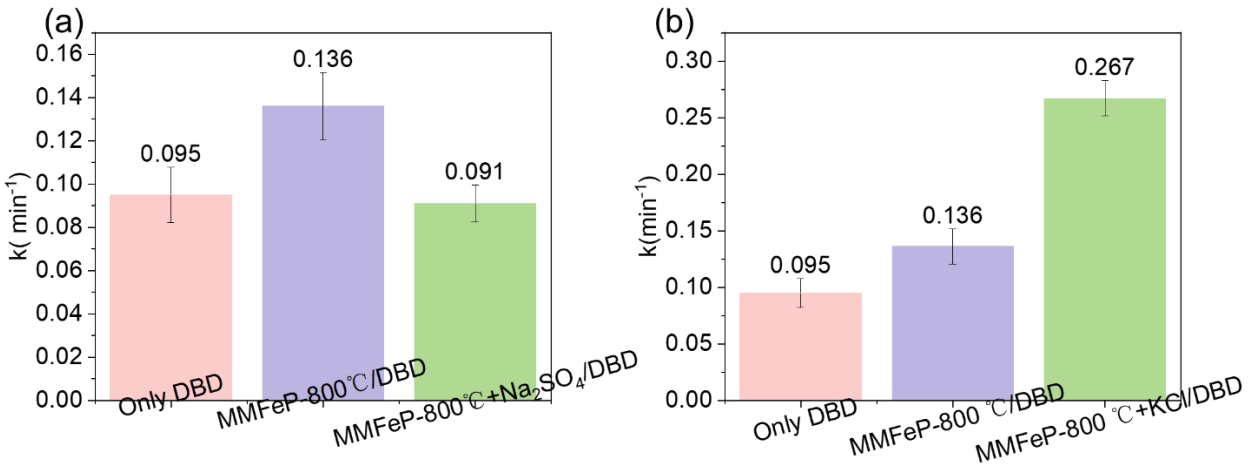


Fig. S13 Reflected rates under DBD alone and with MMFeP-800 ℃, (a) Na_2SO_4, (b) KCl.

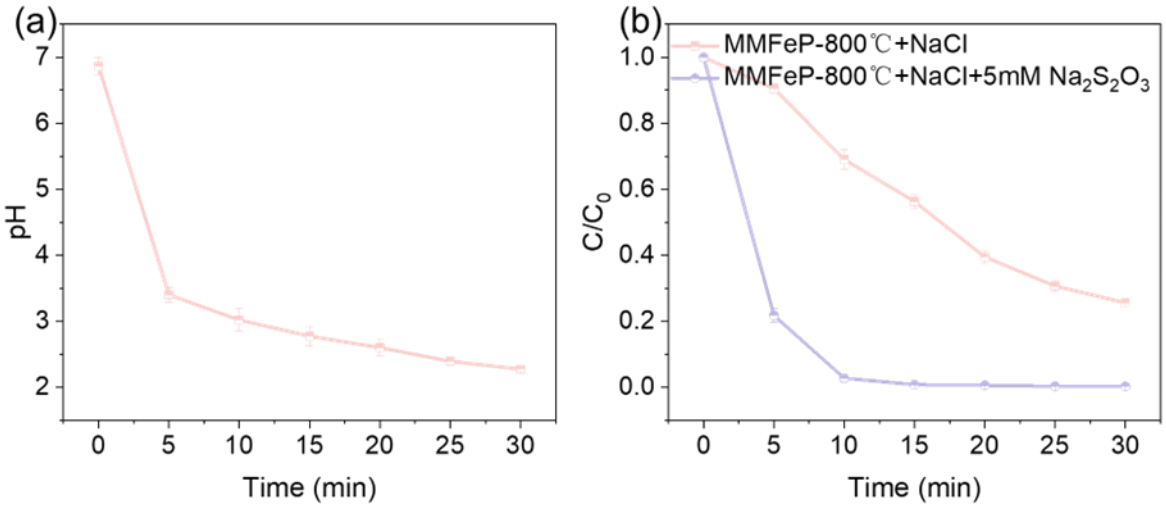


Fig. S14 (a) The change of pH during the reaction in NaCl, (b) Effects of bursting agents $Na_2S_2O_3$

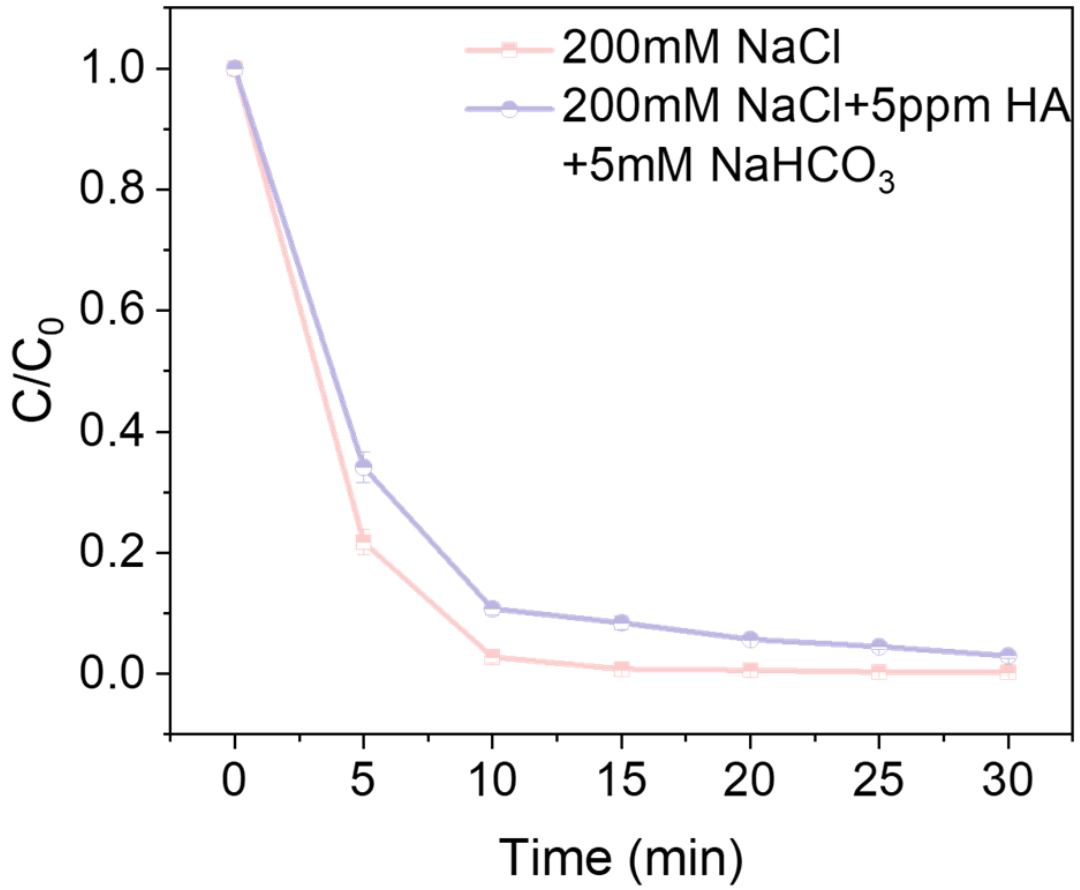


Fig. S15 Effect of 5 mM HA and 5 mM $NaHCO_3$ on the degradation of SMT.

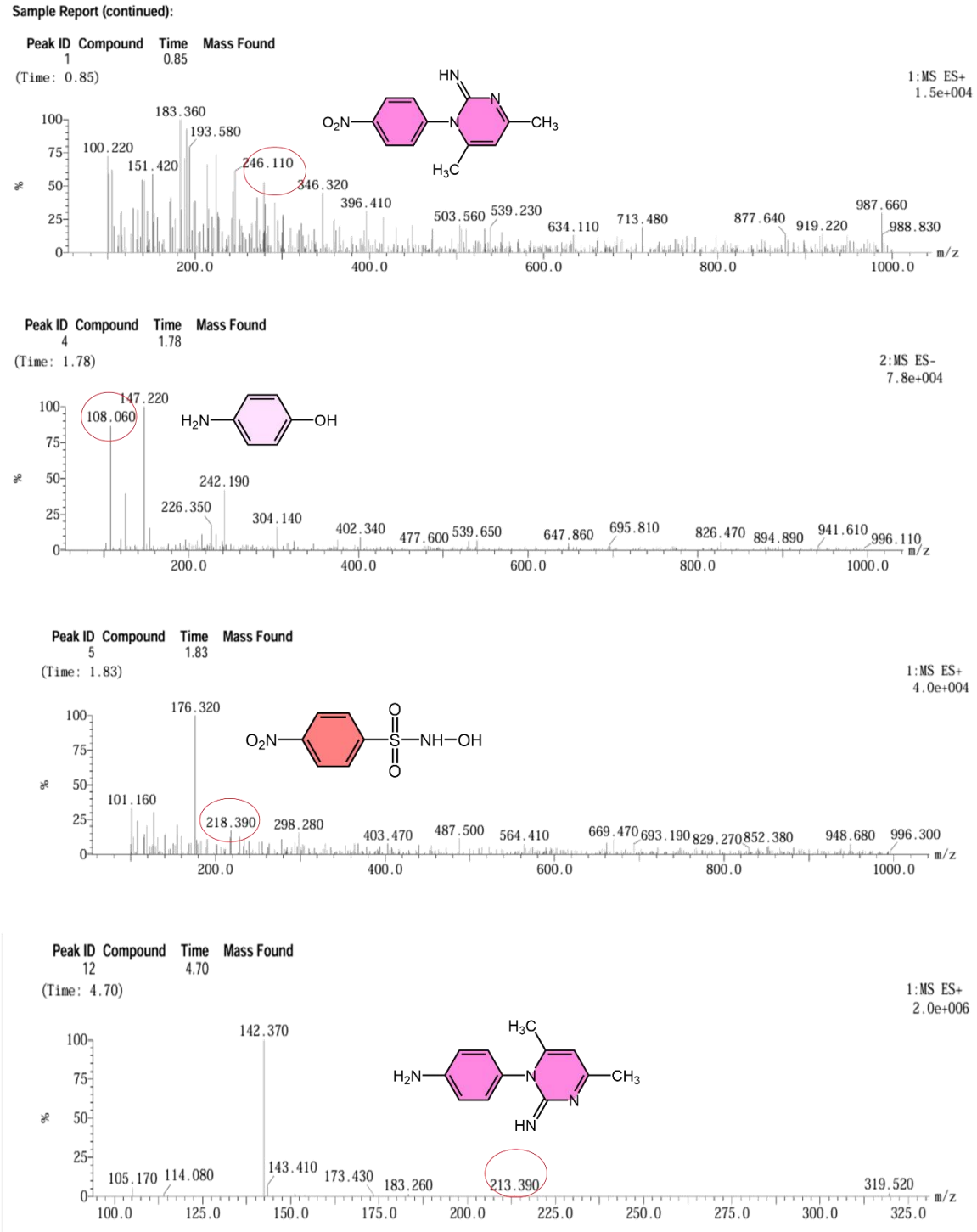


Fig. S16 The LC-MS results of intermediates in MMFeP-800 ℃/NaCl/DBD.

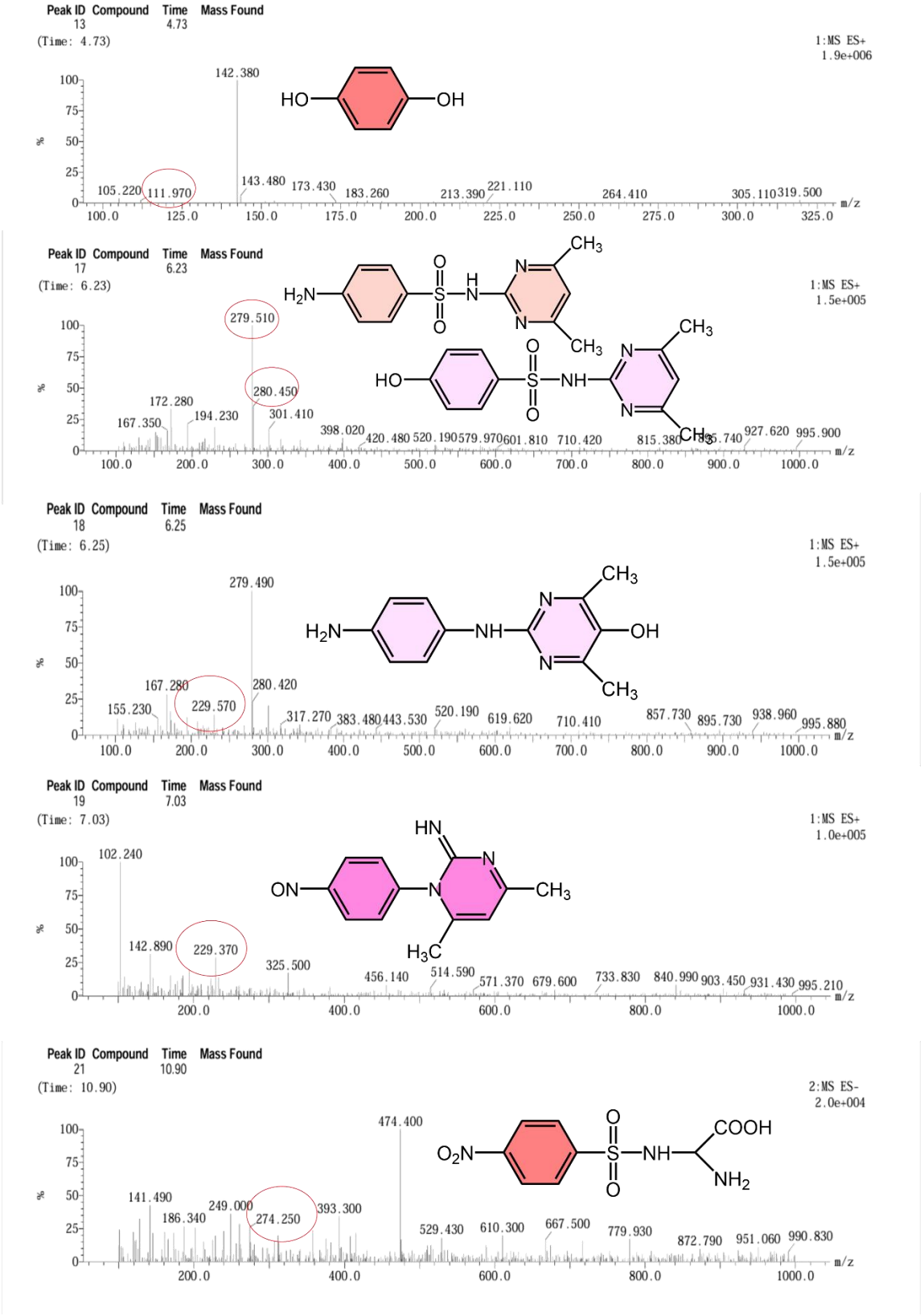


Fig. S17 The LC-MS results of intermediates in MMFeP-800 ℃/NaCl/DBD.

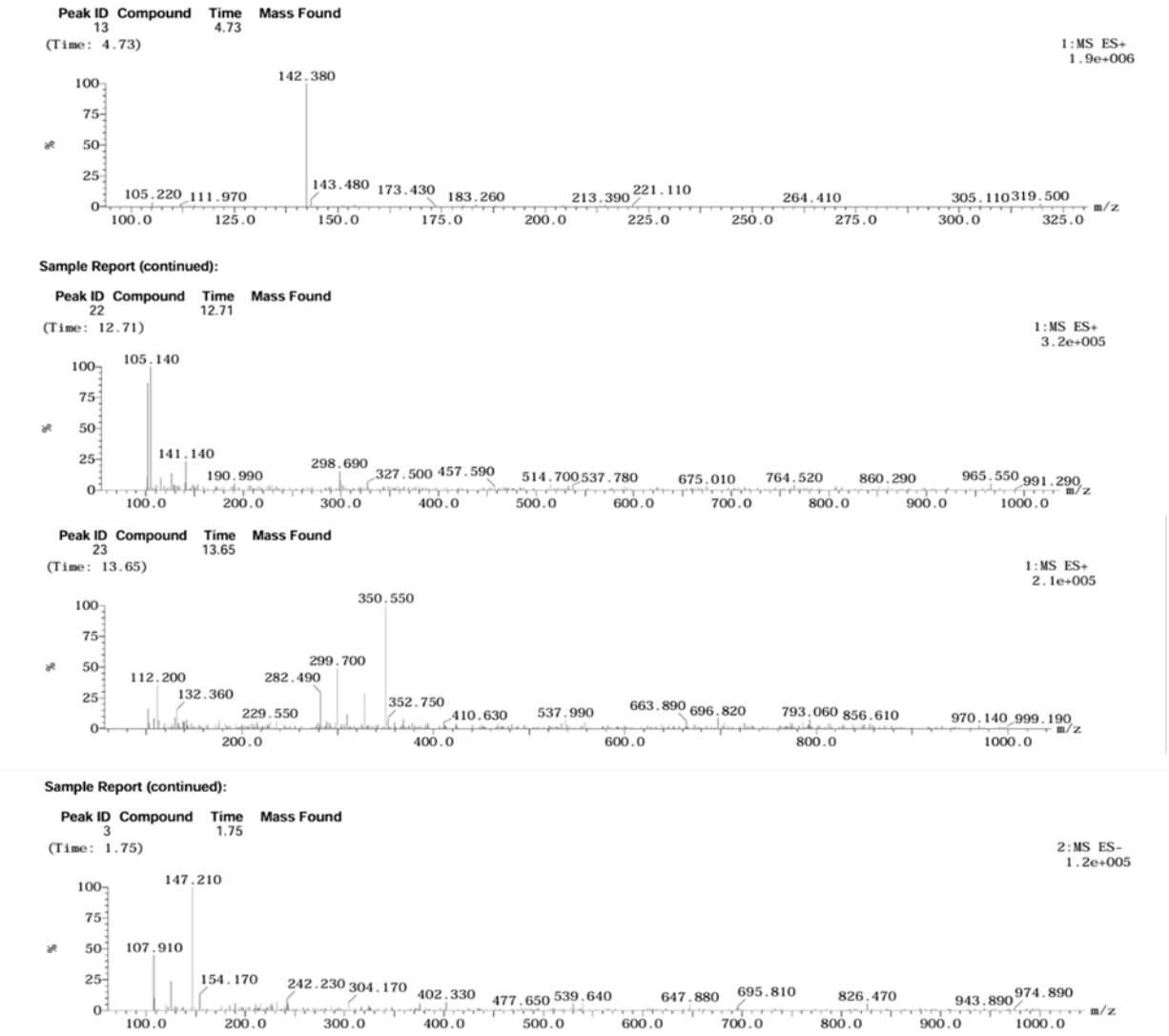


Fig. S18 The LC-MS results of major retention times.

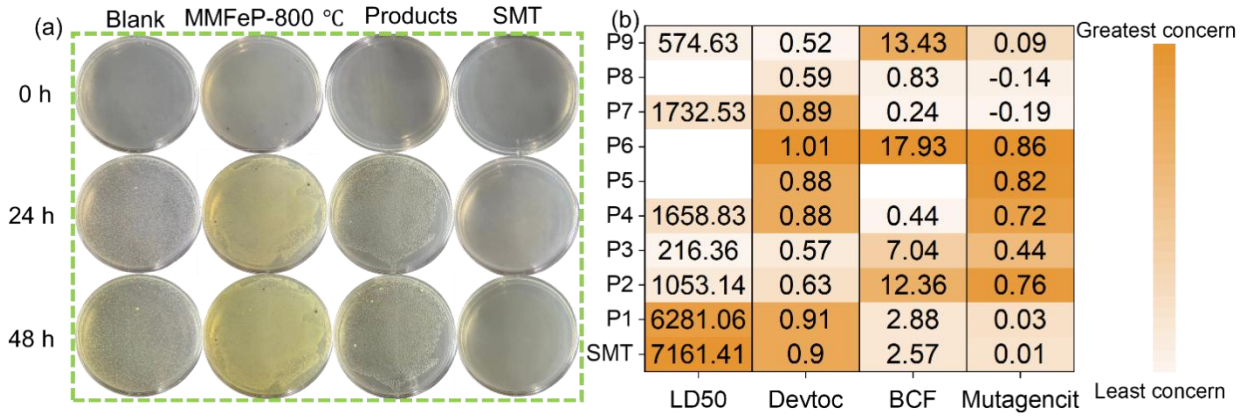


Fig. S19 (a) The digital images of the antibacterial experiment blank, undegraded SMT, catalyst MMFeP-800 ℃, and degraded SMT products; (b) Toxicity prediction of SMT and its degradation intermediates.

A J C, A Y X, A Y W, A D X, A W S, B Y Z, A M L, A J A (2021). Degradation of tetracycline hydrochloride in aqueous via combined dielectric barrier discharge plasma and Fe–Mn doped AC. Chemosphere, 138141

Du C, Zhang L, Wang J, Zhang C, Li H, Xiong Y (2010). Degradation of Acid Orange 7 by Gliding Arc Discharge Plasma in Combination with Advanced Fenton Catalysis. Plasma Chemistry and Plasma Processing, 30(6): 855-871

Guo H, Li Z, Zhang Y, Jiang N, Wang H, Li J (2020). Degradation of chloramphenicol by pulsed discharge plasma with heterogeneous Fenton process using Fe3O4 nanocomposites. Separation and Purification Technology, 253: 117540

Shao F, Wang Y, Mao Y, Shao T, Shang J (2020). Degradation of tetracycline in water by biochar supported nanosized iron activated persulfate. Chemosphere, 261::127844